Case Studies in Construction Materials 19 (2023) e02622

Contents lists available at ScienceDirect

Case Studies in Construction Materials

journal homepage: www.elsevier.com/locate/cscm

Case study

Machine learning models for predicting rock fracture toughness at different temperature conditions

Xunjian Hu [a], Dong Liao [b,*], Dongdong Ma [c,d], Senlin Xie [a], Ni Xie [e], Haibo Hu [a], Xiaonan Gong [a]

[a] *Research Center of Coastal and Urban Geotechnical Engineering, Zhejiang University, Hangzhou 310058, China*
[b] *Department of Civil and Environmental Engineering, The Hong Kong Polytechnic University, Kowloon 100872, China*
[c] *State Key Laboratory for Geomechanics and Deep Underground Engineering, China University of Mining and Technology, Xuzhou 221116 China*
[d] *School of Mechanics and Civil Engineering, China University of Mining and Technology, Xuzhou 221116 China*
[e] *Faculty of Engineering, China University of Geosciences (Wuhan), Wuhan 430074, China*

A R T I C L E I N F O

Keywords:
Machine learning
Fracture toughness
Rock mechanics
Temperature
Semi-circle bend test

A B S T R A C T

The rock fracture toughness (RFT) is significantly influenced by thermal treatments. Accurate evaluation of RFT at different temperatures holds great importance in the fields of geotechnical engineering. Current analytical and empirical models, based on our current but incomplete understanding of the fracture mechanics theory, are unable to produce a priori predictions of RFT. As a result, researchers have to rely on experiments, which are often costly and time-consuming, to understand external environment, internal factors and RFT links in rocks. This research explores the potential of employing machine learning (ML) models as an effective approach to address such challenges. Six ML models are presented, including support vector machine (SVM), random forest (RF), back propagation neural network (BPNN), back propagation-particle swarm optimization (BP-PSO), convolutional neural network (CNN), and radial basis function neural network (RBF). These models are applied using a dataset of 297 samples derived from previous studies involving semi-circle bend tests. The dataset encompasses 15 input variables, including sample radius, sample thickness, notch length, support span, inclination angle of the notch, tensile strength, uniaxial compressive strength, density, quartz content, feldspar content, gypsum content, clay content, other minerals, loading rate, and temperature. The results of three statistical metrics (root mean square error (RMSE), coefficient of determination (R^2), and mean absolute error (MAE)) confirm that the ML models are able to predict the temperature-dependent RFT in modes I, II and III with high accuracy. The results demonstrated that the SVM model shows a better performance than the other five models. In the case of testing dataset, the RMSE, MAE and R^2 values for SVM model are 0.1122 MPa·$m^{1/2}$, 0.0829 MPa·$m^{1/2}$ and 0.9506, respectively. Additionally, feature importance analysis highlights that the temperature and inclination angle are the most influential variables affecting the RFT.

1. Introduction

Understanding the temperature-dependent mechanical behavior of reservoir rocks has become increasingly important in recent

* Corresponding author.
E-mail address: liaodong@zju.edu.cn (D. Liao).

https://doi.org/10.1016/j.cscm.2023.e02622
Received 17 July 2023; Received in revised form 9 October 2023; Accepted 26 October 2023
Available online 26 October 2023

years due to the rising demand for high-temperature applications in geotechnical engineering [1–5]. Rock fracture toughness (RFT), a fundamental mechanical property in rock mechanics, plays a crucial role in characterizing the resistance of rocks to fracture initiation and propagation [6,7]. Accurate measurement of RFT under high-temperatures is therefore of significant importance, as it provides valuable insights into geotechnical engineering, including deep radioactive waste disposal, resource mining, underground coal gasification, safety drilling, and geothermal resource exploitation.

Fracture mechanics theory encompasses a comprehensive understanding of fracture behavior of rocks, delineating three fundamental failure modes: mode I (tension/opening mode), mode II (in-plane shear/sliding mode), and mode III (out-of-plane shear/sliding mode), as illustrated in Fig. 1. With the modes mentioned above, many experimental techniques may be utilized to evaluate RFT using the procedures recommended by the International Society of Rock Mechanics [8]. Many researchers have investigated the RFT under different loading modes [9–11]. However, most of these studies have focused on RFT at room temperature, with only a few considering the influence of temperature [2,6,12–14]. Their experimental findings demonstrate the significant influence of temperature on RFT. For example, Al-Shayea [15] reported a 24% increase in limestone RFT at 116 °C compared to room temperature. Miao et al. [2] observed a decreasing trend in RFT of granite with increasing temperature from 25°C to 300°C due to thermal treatment. Alneasan and Alzo'ubi [6] showed that RFT is directly proportional to the temperature when the temperature between room temperature and 250 °C, but decreases significantly with the increase of temperature when the temperature between 250 and 500 °C. One of the primary reasons for the alteration of RFT after high-temperature treatment is the extensive initiation of thermal-induced cracks in the rock. This correlation has been substantiated through laboratory tests utilizing different observation techniques, including scanning electronic microscopy, microscopic thin section and acoustic emission [1,6,7,16,17]. For example, compared to room temperature, elevating the temperature to 250 °C results in isolated and longer thermal fractures, whereas at 500 °C, thermal fractures widen and coalesce into extensive continuous fractures [6]. The development of the fracture process zone is one of the underlying mechanisms explaining the changes in RFT following high-temperature treatment [2,17–19]. The existence of thermally-induced cracks greatly affects the development of fracture process zone in rocks under different loading modes (Fig. 1). Thermally-induced cracks can easily coalesce to form the continuous and long fracture, which leads to the fracture process zone actively develops at a small loading level. Moreover, rocks with a higher density of thermally-induced microcracks exhibit a prolonged duration of fracture process zone development [17]. These observations collectively emphasize the significant impact of temperature on the RFT. Although these laboratory tests have contributed to an in-depth understanding of the temperature-dependent RFT, they entail substantial investments in terms of time, resources, and the complexity of laboratory measurements. Sample preparation procedures, the need for precise and sensitive instrument setups, and the limited availability of a large number of cores pose challenges in conducting temperature-dependent RFT measurements in the laboratory [20,21].

In the field of rock mechanics, the limited amount of data obtained from experimental tests constrains the comprehensive investigation of reservoir fracture characteristics. To address this challenge, various empirical equations and theoretical criteria have been proposed for RFT prediction in geotechnical engineering practice. For example, previous studies by Chang et al. [9] and Roy et al. [22] have made notable progress in establishing correlations between RFT and physical properties. However, empirical equations usually have poor accuracy. The works of Wei et al. [23,24] also showed that the apparent fracture toughness of small-scale rock samples is significantly dependent on sample geometry and size. Furthermore, RFT is influenced by numerous factors, including temperature and loading rate, which are difficult for empirical equations to fully incorporate [15,25]. Additionally, rock type has a significant impact on the relationships, but empirical equations or theoretical criteria have not been able to accommodate it. Such limitations necessitate the development of alternative and more effective tools capable of predicting RFT at varying temperatures and further advancing our understanding of temperature-dependent RFT.

As a valuable complementary approach, machine learning (ML) based models have been successfully used in a wide range of geotechnical engineering [26,27]. Within this context, the prediction of strength properties has garnered significant attention [21, 28–33]. ML as a statistical modeling technique identifies hidden and unknown relations between parameters of a given experimental database without any physics knowledge [32]. Rock is a natural heterogeneous material, and its mechanical properties are affected by many internal and external factors. Therefore, ML has unique advantages for predicting the mechanical properties of rocks. Notably, ML-based models have been employed for the accurate estimation of RFT in recent studies [20,34–40]. Table 1 summarizes the main research efforts in the field of RFT prediction. However, the ML techniques have rarely been used to solve problems related to temperature, and it is more valuable but still not reported to integrate ML techniques with thermo-mechanical coupling analyses to facilitate the prediction of fracture toughness of rocks after high-temperature treatment. Furthermore, few studies have explored the

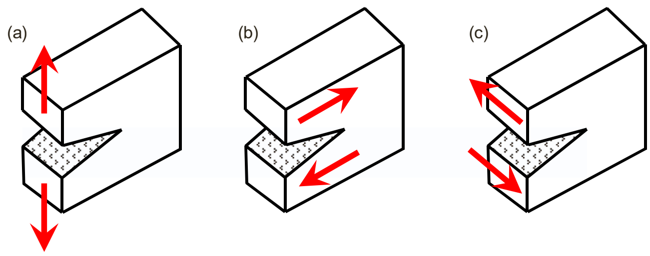

Fig. 1. Three basic failure modes in rock material. a mode I (tension/opening mode); b mode II (in-plane shear/sliding mode); c mode III (out-of-plane shear/sliding mode). Note: the red arrows represent the direction of movement.

Table 1
Applications of ML models for RFT prediction.

References	Input variables	Output variables	Model numbers	Sample numbers	Variable ranking	Remarks
Roy et al.[20]	TS, V_P, V_S, ρ	K_{IC}	4	46	No	This is the first time the soft computing method has been applied to RFT prediction.
Wang et al.[34]	TS, R, B, α_0, α_1, α_B	K_{IC}	4	8888	No	Numerical simulation is adopted to enrich the number of datasets. The random regression forest is more suitable to predict mode I RFT.
Afrasiabian and Eftekhari[35]	UCS, BTS, E	K_{IC}	2	60	Yes	It found that simple basic available rock properties are enough to develop reliable prediction models.
Dehestani et al.[36]*	MT, EM, FM, D, t, c, α, TS	K_{IC}, K_{IIC}, K_{eff}	20	401	No	This study provides a ML-based model for the prediction of RFT and fracture load using a wide range of data points.
Emami Meybodi et al.[37]	TS, UCS, E	K_{IC}, K_{IIC}	4	24	No	The K-fold cross-validation was a beneficial method for determining the model with the best performance for prediction.
Mahmoodzadeh et al.[38]	R, B, α_1, α_B, α_s, TS	K_{IC}	7	250	Yes	Developing support vector regression-particle swarm optimization algorithms to predict mode I RFT.
Mahmoodzadeh et al.[39]*	MT, EM, TS, D, t, a, α	K_{IC}, K_{IIC}, K_{eff}	12	1715	Yes	Material type (MT) has shown the most significant impact on the RFT.
Lawal and Kwon[40]	V_P, V_S, ρ	K_{IC}	2	43	No	They adopted simple parameters and still achieved more accurate prediction results.

Note: *A variety of materials, including rock and concrete, were included in the work by Dehestani et al. [36] and Mahmoodzadeh et al. [39]. TS: tensile strength; V_P: P-wave velocity; V_S: S-wave velocity; ρ: density; R: sample radius; B: sample thickness; a_0: initial length of notch; a_1: final length of crack, R_s: the radius of incision of the Chevron notch; α_0: a_0/R; α_1: a_1/R; α_B: B/R; α_s: R_s/R; UCS: uniaxial compressive strength; BTS: Brazilian tensile strength; E: modulus; MT: material type; EM: experimental method; FM: fracture mode; D: diameter; t: thickness; c: half-notch length; α: inclination of the notch with loading direction; K_{IC}: mode I RFT; K_{IIC}: mode II RFT; K_{eff}: effective RFT in mode III; RFT: rock fracture toughness.

ranking of input variables in RFT prediction [35,39]. Additionally, the existing ML-based models often consider a limited range of input variables (Table 1). For example, the effect of mineralogical composition on the RFT under high temperature condition is ignored [41]. ML-based models have advantages to examine extrinsic (e.g., temperature, loading rate) and intrinsic (e.g., mineralogical composition, density) factors influencing the RFT, which may not be readily considered or controlled using the empirical equations, theoretical criteria and experimental tests.

The primary objective of this work is to develop ML-based models capable of predicting the temperature-dependent RFT and to investigate the influence of input variables on RFT. To achieve this, a comprehensive dataset comprising 297 samples has been compiled from relevant literature sources, encompassing the physical, geometric, mechanical, environmental, and mineralogical properties of the samples. Subsequently, six ML models, namely support vector machine (SVM), random forest (RF), back propagation neural network (BPNN), back propagation-particle swarm optimization (BP-PSO), convolutional neural network (CNN), and radial basis function neural network (RBF), are trained using this dataset. Through rigorous evaluation, the model with the highest performance is identified, and the ranking of input variables is determined. Furthermore, three key aspects are discussed: (a) the crucial factors influencing prediction accuracy, (b) the necessity of ML model input variables for predicting temperature-dependent RFT and

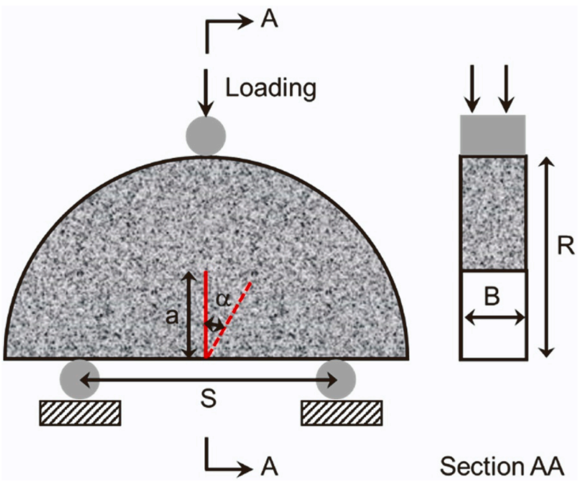

Fig. 2. SCB specimen under three points bending test. a notch length; α inclination angle of notch; R sample radius; B sample thickness; and S support span.

(c) future works.

2. Methodology

2.1. Data collection and preprocessing

In order to estimate the temperature-dependent RFT, a total of 297 samples were collected following the guidelines outlined by the International Society of Rock Mechanics [8] for the semi-circle bend (SCB) test (Fig. 2). The SCB test is a widely adopted method for assessing the RFT under various modes, including mode I, mode II, and mode III. The samples are collected from various references [1–3,6,14,42–44], considering typical rock types in geotechnical engineering, including granite, sandstone, mudstone, and gypsum rock. According to the literature and data availability, 15 input variables are considered, including sample radius (R), sample thickness (B), notch length (a), support span (S), inclination angle (α), tensile strength (TS), uniaxial compressive strength (UCS), density (ρ), quartz content (C_Q), feldspar content (C_F), gypsum content (C_G), clay content (C_C), other mineral (C_O), loading rate (v) and temperature (T). The output variable of ML models is the RFT (K_C). Some physical or mechanical properties, which are unavailable in the original sources, are collected from secondary sources [45–47]. Among of the total 297 samples, 80% were randomly selected for training the predictive ML-based models, while the remaining 20% were used to test the performance of the developed ML-based models in predicting the RFT based on the 15 input variables. The statistical parameters for both the training and testing datasets are provided in Table 2. It should be noted that the calculation of the RFT under mode III in this work is based on the effective stress intensity factor [12]. Therefore, in this work, the output data include modes I, II and III RFT.

2.1.1. Box plot representation

The box plot serves as a visual summary of the statistical characteristics of the dataset. Statistical analyses were performed on key parameters such as maximum and minimum values, variance, mean, and quartiles to investigate the influence of rock properties, comprising 15 input variables and RFT, as depicted in Fig. 3.

Currently, the RFT at room temperature predicted by ML models mainly focuses on the pure mode I or pure mode II RFT [20,34,35,37,38–40]. Due to the uncertainty of the direction of flaws in rocks, the fracture with a mixed mode tends to occur. As a result, there is growing interest among scholars in predicting the RFT at room temperature under mode III conditions using ML models [39]. However, none of the aforementioned works considered the effect of temperature. Therefore, this work aims to address this gap by encompassing a range of inclination angles of the notch, spanning from 0° to 55°. As a result, the experimentally measured RFT in this

Table 2
Statistics analysis of the training and testing datasets.

	Properties	Average	Standard deviation	Minimum	Maximum	Median
Training dataset (237)	R (mm)	33.65	15.02	25.00	75.00	25
	B (mm)	23.16	6.12	20.00	35	20
	a (mm)	15.78	6.33	8.33	28	12.5
	S (mm)	60.71	9.98	40	90	61
	α (°)	12.34	19.31	0	55	0
	T (°C)	321.69	219.00	20	800	300
	TS (MPa)	6.77	2.98	2.1	11.63	5
	UCS (MPa)	72.59	54.89	21	174.78	33
	ρ (g/cm^3)	2.62	0.17	2.13	2.79	2.65
	C_Q (%)	43.81	25.32	0	71	65
	C_F (%)	19.29	25.64	0	70	5
	C_G (%)	7.21	23.74	0	85.4	0
	C_C (%)	5.05	20.95	0	92	0
	C_O (%)	24.14	16.17	0	59.15	30
	v (mm/min)	0.23	0.39	0.012	1.00	0.012
	K_C ($MPa{\cdot}m^{1/2}$)	0.78	0.43	0.04	2.21	0.78
Testing dataset (60)	R (mm)	36.67	14.77	25	75	25
	B (mm)	25.50	7.23	20	35	20
	a (mm)	17.58	6.68	8.33	28	12.5
	S (mm)	60.68	8.47	40	90	61
	α (°)	15.50	20.77	0	55	0
	T (°C)	310.58	206.42	20	700	300
	TS (MPa)	6.98	3.05	2.10	11.63	5.00
	UCS (MPa)	82.07	53.94	21.00	174.78	33.00
	ρ (g/cm^3)	2.65	0.16	2.13	2.79	2.65
	C_Q (%)	39.69	24.77	0	71	29
	C_F (%)	26.27	29.86	0	70	5
	C_G (%)	5.69	21.30	0	85.4	0
	C_C (%)	7.67	25.43	0	92	0
	C_O (%)	20.28	15.79	0	59.15	29
	v (mm/min)	0.38	0.47	0.012	1.00	0.031
	K_C ($MPa{\cdot}m^{1/2}$)	0.84	0.49	0.03	2.08	0.86

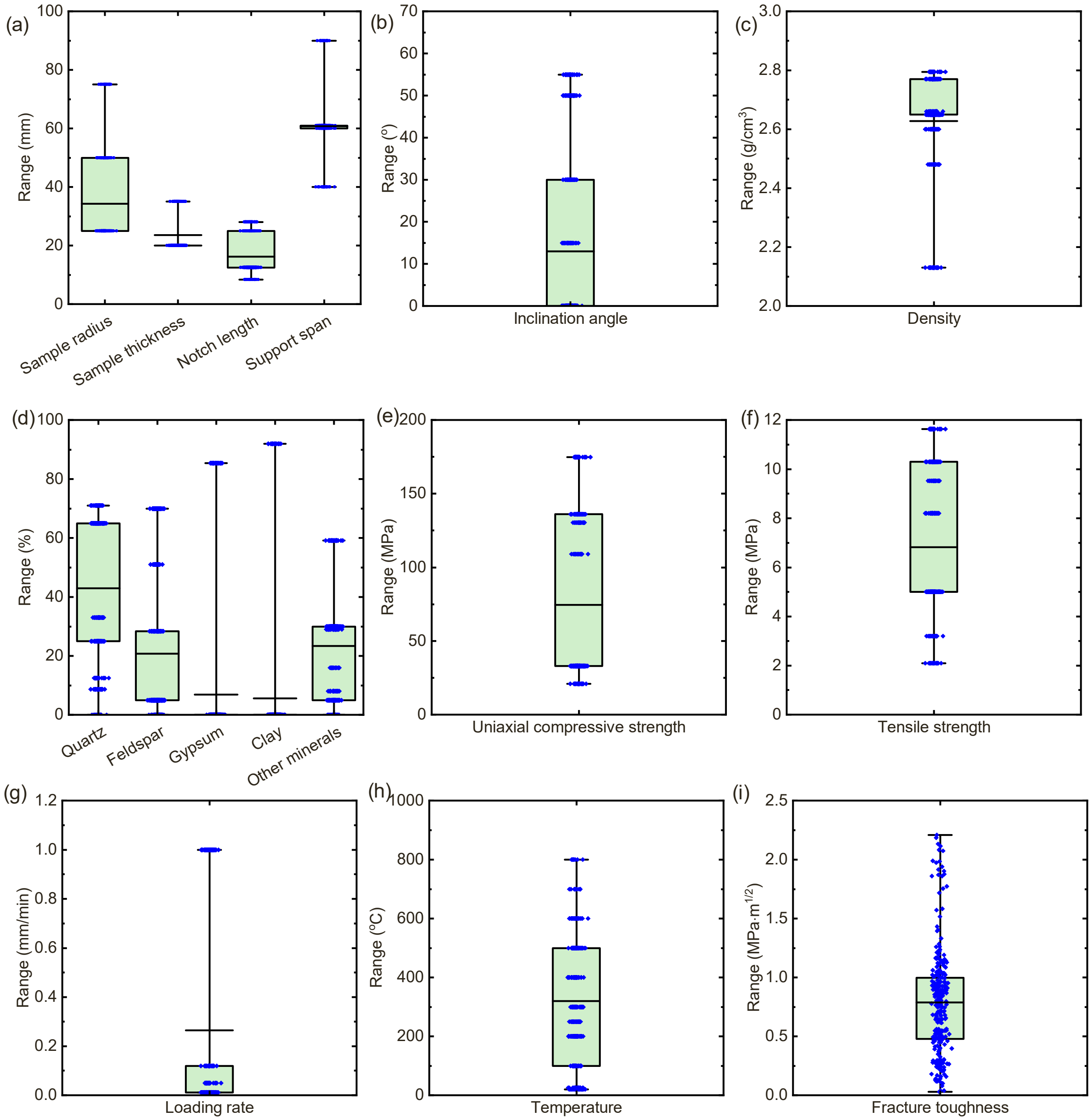

Fig. 3. Box plot for statistical analysis. a sample radius, sample thickness, notch length and support span; b inclination angle of notch; c density; d the content of quartz, feldspar, gypsum, clay and other minerals; e uniaxial compressive strength; f tensile strength; g loading rate; h temperature; i rock fracture toughness.

study encompasses three distinct fracture modes: mode I, mode II, and mode III [13]. Consequently, a dataset with a more comprehensive range is adopted.

The temperature ranges from room temperature to 800 °C, which includes the most favorable reservoir temperature range for enhanced geothermal systems [48]. In addition, the uniaxial compressive strength, tensile strength, density and loading rate range from 21 MPa to 174.78 MPa, 2.1 to 11.63 MPa, 2.13 g/cm^3 to 2.80 g/cm^3, 0.01 mm/min to 1 mm/min respectively. The value of RFT ranges from 0.03 MPa·m$^{1/2}$ to 2.21 MPa·m$^{1/2}$. The maximum RFT is almost 73.6 times that of the minimum ones.

2.1.2. Pearson correlation

The Pearson correlation coefficient was employed as a vector similarity metric to assess the statistical correlation and understand the relationship between the input and output variables prior to modeling [31]. Fig. 4 shows the Pearson correlation within 15 input variables and RFT. The RFT exhibits a positive Pearson correlation coefficient with the uniaxial compressive strength, tensile strength, density, feldspar content, and loading rate, while it displays a negative correlation with temperature. The sample radius, notch length and content of quartz are not closely associated with the RFT. In addition, due to the SCB test requirements [8], the sample radius and the other three geometric properties (sample thickness, notch length and support span) show a strong correlation. Nevertheless, the temperature exhibits weak correlation with the remaining 14 input variables, given that they are all influenced by the physical, mechanical properties, or loading conditions of a sample.

2.2. Model performance assessment

This study utilizes three statistical indicators to assess the performance of six ML models. The indicators are root mean square error (RMSE), coefficient of determination (R^2), and mean absolute error (MAE). The mathematical expressions for the three performance indices are provided below [31]:

$$\mathrm{RMSE} = \sqrt{\frac{1}{n}\sum_{i=1}^{n}\left(y_i - y_i^*\right)^2} \tag{1}$$

$$\mathrm{R}^2 = 1 - \frac{\sum_{i=1}^{n}\left(y_i - y_i^*\right)^2}{\sum_{i=1}^{n}\left(y_i - \overline{y}\right)^2} \tag{2}$$

$$\mathrm{MAE} = \frac{1}{n}\sum_{i=1}^{n}\left|y_i^* - y_i\right| \tag{3}$$

where n represents the number of data points, y_i and y_i^* are measured and predicted values, $\overline{y}$ represents the means of the measured

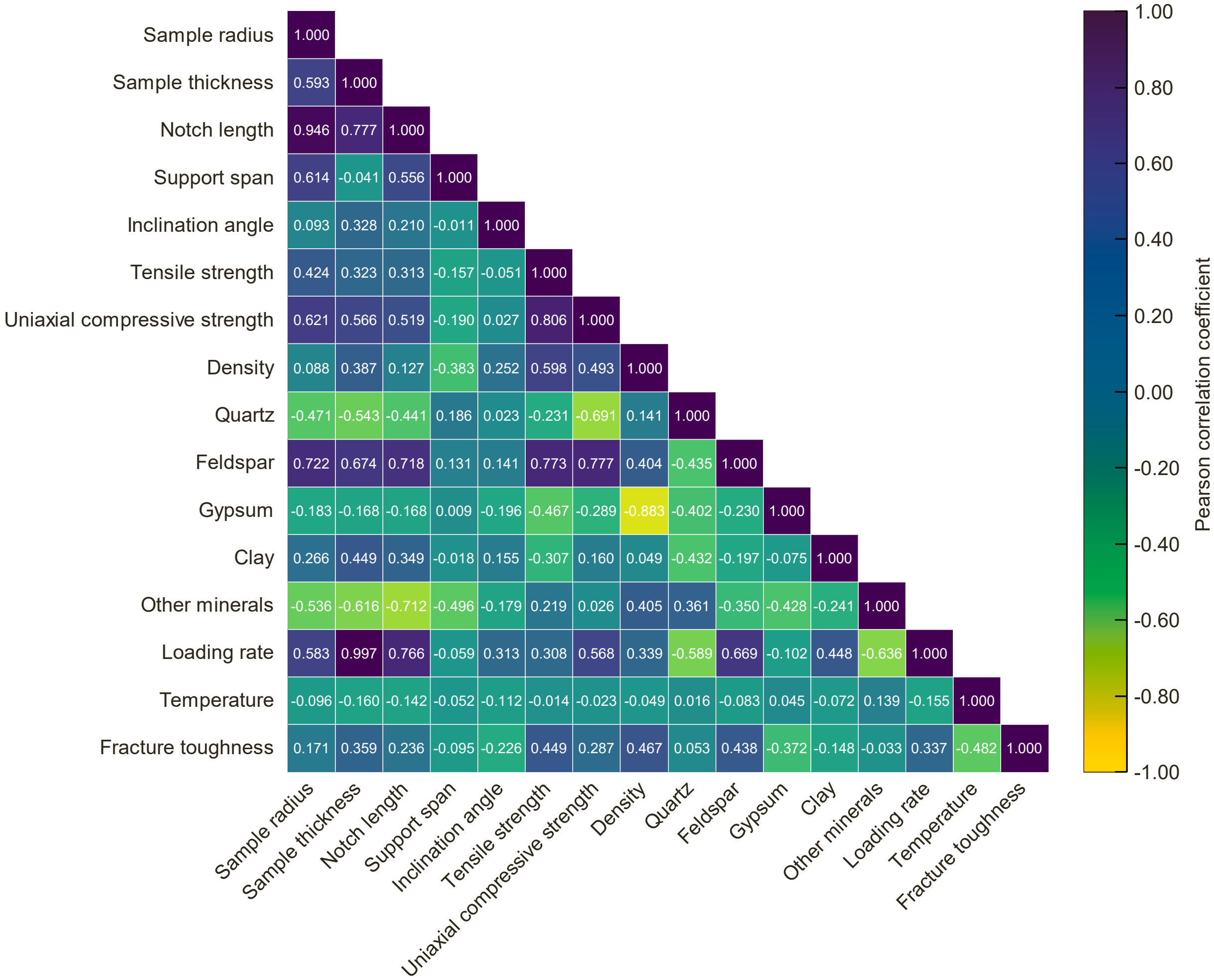

Fig. 4. Pearson correlation within 15 input variables and rock fracture toughness. A coefficient of 1 signifies a robust positive correlation, whereas a coefficient of − 1 indicates a pronounced negative correlation.

values.

2.3. Machine learning models

Numerous ML-based models have been proposed in previous studies, making it unfeasible to comprehensively analyze all available models within a single research investigation. Previous studies have identified the most prevalent ML models known for their favorable performance [27,31,49,50]: SVM, CNN, RF, BPNN, BP-PSO, and RBF. While these ML models have demonstrated commendable performance, each model has its own merits, limitations, and can yield diverse outcomes. Given that the selection of the optimal ML model predominantly hinges on the research problem and available data [27], the subsequent paragraphs briefly expound upon the characteristics of each ML model.

The SVM, rooted in statistical learning theory and founded upon the principle of structured risk minimization, operates by transforming the input space into a higher-dimensional representation. Its objective is to identify a hyperplane capable of elucidating the intricate non-linear relationship between input and output variables. During the training process, the SVM diligently minimizes the sum of distances between the hyperplane and the data points, ultimately deriving the optimal hyperplane configuration.

The CNN, a common architecture in deep neural networks, share similarities with traditional neural networks in their layered structure. However, CNNs uniquely exploit local connectivity and shared weights to effectively reduce the number of trainable weights, leading to improved efficiency in weight training and reduced computational memory requirements for training and running the network [49]. A typical CNN architecture consists of several distinct layers, including the convolutional layer, down-pooling layer, and fully connected layer.

The RF, a proficient ensemble learning methodology comprising an amalgamation of multiple decision trees, finds utility in addressing regression problems [51]. Each decision tree, within the RF framework, partitions a root node into leaf nodes through a split function, thereby producing an output variable. The RF generates predictions by aggregating the output variables from these decision trees.

The BPNN, an algorithm characterized by its multi-layered feedforward architecture, entails a sequential two-step computational process encompassing forward propagation and backpropagation. These iterative steps continue until the errors between predicted outputs and actual values diminish below a predefined tolerance threshold. The BPNN configuration comprises an input layer, one or more hidden layers, and an output layer. BPNN use differentiable activation functions like sigmoid or ReLU in their hidden layers.

Particle Swarm Optimization (PSO), a stochastic optimization algorithm rooted in swarm intelligence, operates by orchestrating cooperative and competitive interactions among individuals within a collective group. Each position of particle in the search space represents the parameters to be optimized. Throughout the search process, particles continuously adapt their velocity and position by assimilating their own flight experience, incorporating inertial learning, and incorporating information gleaned from other particles, eventually converging towards the optimal position. In the context of BP-PSO, the PSO algorithm assumes the responsibility of adjusting the weights and biases of BPNN.

The RBF neural network consists of three layers: the input layer, hidden layer with radial basis functions, and output layer. The input layer distributes the input vector coordinates to each unit within the hidden layer. Each unit in the hidden layer generates an activation by utilizing the associated radial basis function. Lastly, each unit in the output layer calculates a linear combination of the hidden unit activations. RBF neural networks and BPNNs have distinct architectures, activation functions, training methods [31].

The aforementioned six ML models encompass various hyperparameters that can significantly influence the predicted outcomes. Consequently, optimizing these hyperparameters is essential to achieve optimal performance for the ML models. The hyperparameters of the ML models are optimized through an iterative trial-and-error process, following an approach that aligns with that of

Table 3
Adopted hyperparameters of the ML models.

ML models	Hyperparameters	Values
SVM	Epsilon	0.01
	cost	4.0
	gamma	0.8
CNN	Batch size	30
	Epochs	100
	Initial learning rate	0.01
	Kernel size	3×1
RF	Number of decision trees	1000
	Minimum leaf size	2
BPNN	number of iterations	3000
	convergence error	0.0001
	learning rate	0.01
BP-PSO	number of iterations	3000
	convergence error	0.0001
	learning rate	0.01
	First weight factor	4.5
	Second weight factor	4.5
	iteration number	30
RBF	Spread of radial basis functions	10

Mahmoodzadeh et al. [39]. The adopted hyperparameters are summarized in Table 3. Data analysis and ML model implementation were conducted using MATLAB (R2020b) or Python on a PC equipped with an Intel(R) Xeon(R) CPU E5–1620 v3 @ 3.50 GHz and 16 GB RAM.

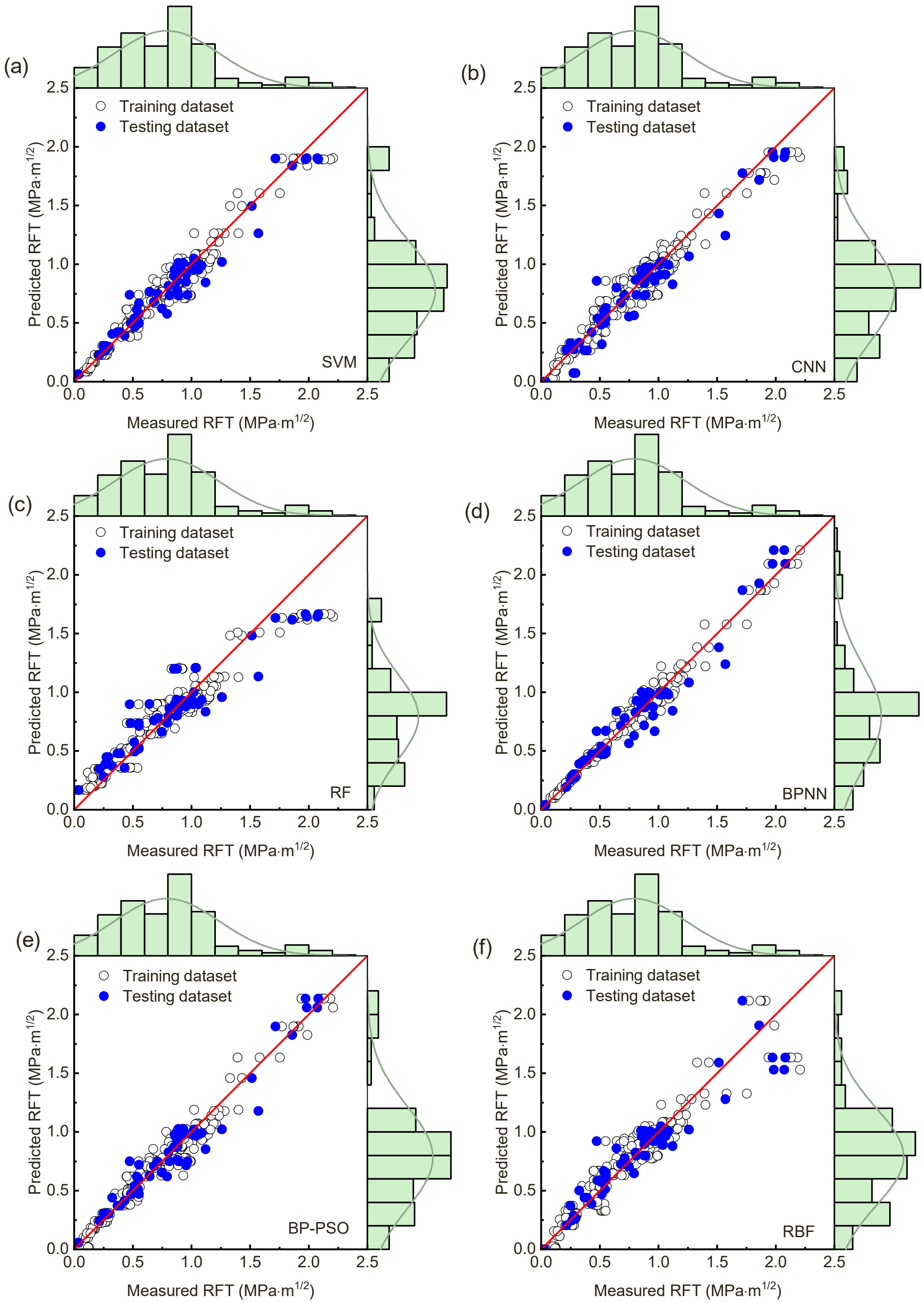

Fig. 5. Correlation between the measured and predicted RFT values of six ML models. a SVM-based model; b CNN-based model; c RF-based model; d BPNN-based model; e BP-PSO-based model; f RBF-based model.

3. Results

3.1. Comparative analysis of different models

The six ML-based models were trained using a randomly selected set of 237 samples from 297 samples. The remaining 60 samples were then used to validate the models, and the three performance indicators (R^2, RMSE, and MAE) were computed. The correlation plot of the measured and the predicted RFT using the SVM, CNN, RF, BPNN, BP-PSO, and RBF models are shown in Fig. 5. Data points situated on or near the diagonal red line indicate a correspondence between the predicted and measured RFT. The data points with a small deviation from the diagonal red line are mainly distributed in the region less than 1.25 MPa·m$^{1/2}$. Because the data points are densely distributed in this region, as shown in the histograms next to the upper and right axes (Fig. 5). However, there are very few data points in the range of 1.25–2.5 MPa·m$^{1/2}$. This also makes the predicted and measured values not clustered near the diagonal red line. It indicates that the amount of data points is critical for the accuracy of ML prediction. Especially the RBF model has poor predictive performance in the high value of RFT interval (1.25–2.5 MPa·m$^{1/2}$), as shown in Fig. 5f. Therefore, it is not recommended to use the RBF model to predict the RFT at high temperatures. In general, the SVM, CNN, RF, BPNN, and BP-PSO models exhibit reliability in predicting the temperature-dependent RFT, as evidenced by the close distribution of data points to the diagonal red lines (Fig. 5a∼e).

Table 4 presents the values of R^2, RMSE, and MAE obtained from both the training and testing datasets for the six ML-based models. Among the ML-based models, the best performing model on the training dataset is BPNN in terms of the highest R^2 value (0.9788) and lowest RMSE value (0.0631 MPa·m$^{1/2}$) and MAE value (0.0444 MPa·m$^{1/2}$). However, the performance of BPNN weakens when applied to the testing dataset, possibly due to its higher dependence on data quantity compared to other ML models in the study of temperature-dependent RFT prediction. For testing dataset, the R^2 value for the SVM model (0.9506) show much higher than other five ML models. At the same time, the RMSE and MAE values show minor differences among the SVM, CNN, BPNN and BP-PSO models, but the RMSE value for the SVM model are lowest than other five ML models (Table 4). Therefore, it is recommended to adopt the SVM model to predict the temperature-dependent RFT. Additionally, the performance of BPNN and BP-PSO models on the testing dataset is almost the same, which can be verified from the values of the R^2, RMSE and MAE (Table 4). This indicates that the performance of the PSO-optimized BPNN model, in terms of predicting temperature-dependent RFT, has not been significantly enhanced compared to the conventional BPNN model. It is important to note that the conclusion regarding the disparity in predictive performance between the BPNN and BP-PSO models may be biased due to the specific model input variables and dataset size employed in this study. This is because the appropriate geotechnical problem for different models may be different [30]. This finding further suggests that the improvement of algorithms may be limited in improving the prediction performance for geotechnical engineering prediction problems. In contrast to other engineering disciplines, geotechnical engineers encounter highly non-linear challenges associated with temperature, time, and moisture dependence, which lead to notable variations in the properties of rocks and soils [26]. Therefore, greater emphasis should be placed on selecting appropriate input variables and recognizing the significance of the geotechnical engineering problem under investigation.

3.2. Feature importance analysis

Shapley additive explanations (SHAP) belong to the class of additive feature attribution methods, providing a quantification of the contribution of the feature to a prediction. This approach is based on the unification of game theory and local explanations [52,53]. SHAP unifies global interpretation (for entire datasets) and local interpretation (for individual samples) for a ML model. For a more detailed explanation and computational method of SHAP, please refer to the work of Lundberg and Lee [52] and Wang et al.[53]. For SHAP analysis, the Python package *shap* was used (version 0.37.1). In this work, only the global interpretation of the results of the RF model is conducted. The results predicted by RF can be interpreted by SHAP in different ways. First the feature importance of the input variables, which indicates the general impact of the features on the predictions, is given in Fig. 6a. It is actually calculated as the average of the absolute Shapley values of the entire training dataset. The temperature with a value of 0.19833 is the most important feature, followed by the inclination angle with a value of 0.15622. Based on the mean absolute SHAP values, the temperature and inclination angle of the notch are the most important input variables for predicting the temperature-dependent RFT. Additionally, the content of feldspar (0.13240), tensile strength (0.03582), content of other minerals (0.03183), density (0.02610), loading rate (0.02180), the content of quartz (0.02118) and uniaxial compressive strength (0.02018) also demonstrate varying degrees of importance. The mean absolute SHAP values of the remaining 6 input variables are all below 0.02, which means that they have

Table 4
Comparison of performance metrics of six ML models.

ML models	Training dataset			Testing dataset		
	R^2	RMSE (MPa·m$^{1/2}$)	MAE (MPa·m$^{1/2}$)	R^2	RMSE (MPa·m$^{1/2}$)	MAE (MPa·m$^{1/2}$)
SVM	0.9563	0.0916	0.0663	0.9506	0.1122	0.0829
CNN	0.9476	0.1003	0.0773	0.9393	0.1275	0.0983
RF	0.9158	0.1398	0.1024	0.8840	0.1841	0.1374
BPNN	0.9788	0.0631	0.0444	0.9475	0.1146	0.0848
BP-PSO	0.9581	0.0888	0.0675	0.9447	0.1153	0.0808
RBF	0.9002	0.1369	0.0986	0.8736	0.1746	0.1225

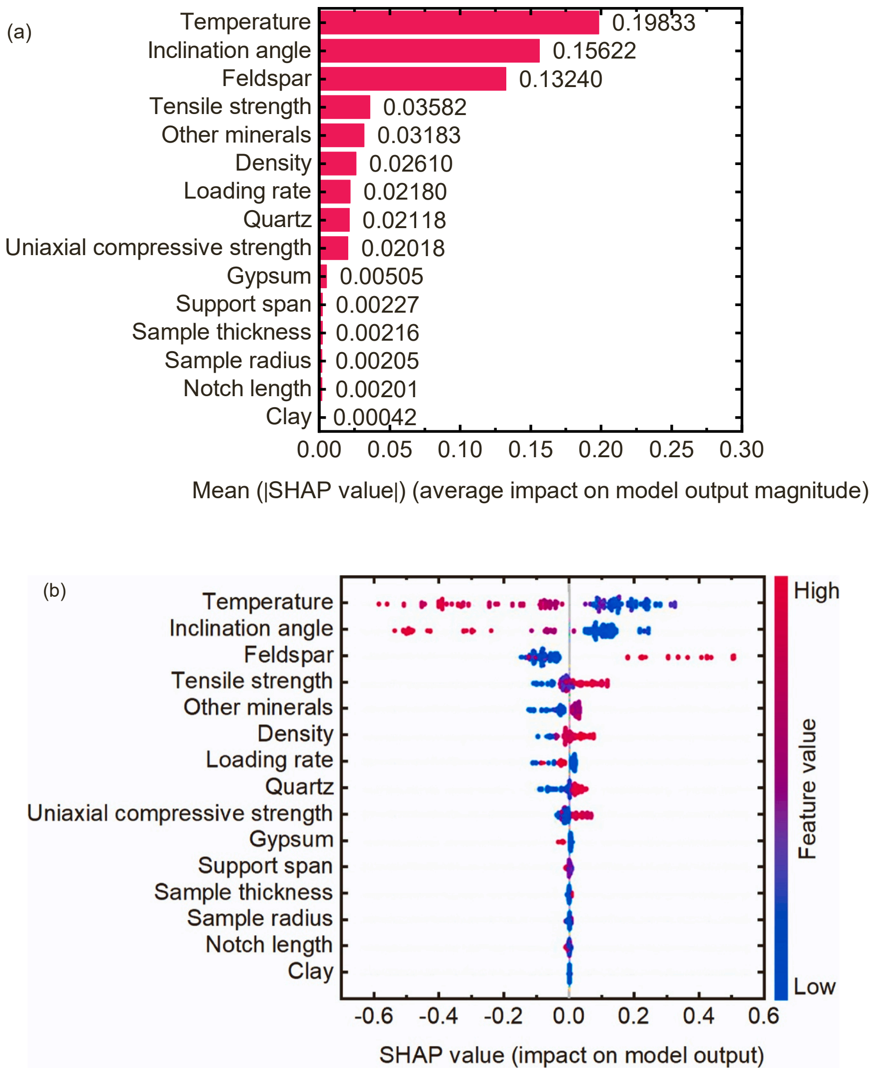

Fig. 6. Global interpretations of RF model by SHAP values. **a** SHAP feature importance; **b** SHAP summary plot. Note: the dots in **b** are the samples in the database, and the color of the dot indicates the value of the specific feature, for which color from blue to red indicates a feature value from low to high.

relatively low impacts on the results. It should be noted that these importance ranking values of the 15 input variables only apply to the rock dataset used in this study and may not be considered a universal rule.

Fig. 6b is a SHAP summary plot of the 15 features, which demonstrates the distribution of the SHAP values for each feature and indicates the corresponding influences trends. For example, the upper left dot in red means a high temperature will lead to a prediction decrease of around 0.6. Therefore, the summary plot not only offers an understanding of which features are important but also how each feature affects RFT. Generally, it is observed that with the increase in the temperature and inclination angle, the RFT will decrease. By contrast, the RFT tends to increase with increasing values for features like the content of feldspar and tensile strength. These plots by SHAP give a global explanation of how the input variables affect the RFT.

To further understand the effect of individual input variables, some input variable is excluded at each time and the remaining input variables are used in six ML-based models. One group completely excludes the mineralogical composition, and the other six groups include 14 input variables and exclude one input variable in turn. The excluded variables, namely temperature, inclination angle, tensile strength, density, uniaxial compressive strength, loading rate, mineralogical composition (the content of quartz, feldspar, clay, gypsum and other minerals), demonstrate their significance in predicting the outcomes, as revealed through the evaluation of feature importance (Fig. 6). Fig. 7 presents the performance metrics (R^2 and RMSE) for the developed groups on the testing dataset. As shown in Fig. 7, for the all six ML models, the R value show remarkable reductions when either temperature or inclination angle is excluded. Conversely, the trend observed in the RMSE values is opposite. These findings align with the observations in Fig. 6 and underscore the crucial role of temperature and inclination angle of the notch in predicting the temperature-dependent RFT. Furthermore, the BP-PSO based model exhibits varying R^2 values ranging from 0.5232 to 0.9503, indicating its sensitivity to the input variables. At the same time, the SVM-based model demonstrates the most favorable predictive performance when sequentially excluding the tensile strength, density, uniaxial compressive strength, loading rate, and mineralogical composition. This is evident from both the R and RMSE values obtained from the testing dataset (Fig. 7).

Interestingly, even after excluding all mineralogical compositions, the ML models consistently achieve high prediction performance when estimating the RFT at different temperatures. This is different from the observation made by Tie et al. [33]. They found that the mineralogical composition is an important input variable in the model training, and the training with different type of rocks can significantly reduce the performance of ML-based models when estimating the rock tensile strength. Such differences may stem from the higher number of input variables employed in this study (15 input variables) compared to the work of Tie et al. (6 input variables) [33]. And this may make the predictive performance of the ML-based models decrease when training with different type of rocks. It is important to note that this does not undermine the importance of mineralogical composition as an input variable for predicting RFT at various temperatures. The mineralogical composition undergoes changes with varying pre-heated treatment temperatures [19], but this aspect is overlooked in the present study, treating the mineralogical composition of rocks at different temperatures as identical. The intricate relationship between mineralogical composition and RFT will be comprehensively discussed in the subsequent section.

4. Discussion

ML-based models demonstrate the potential to effectively tackle complex geotechnical challenges by establishing robust associations between input and output variables, without relying on explicit physical knowledge. However, there are still many factors that affect the accuracy of predictions based on ML models, and ML also has some challenges and limitations in the prediction of RFT after

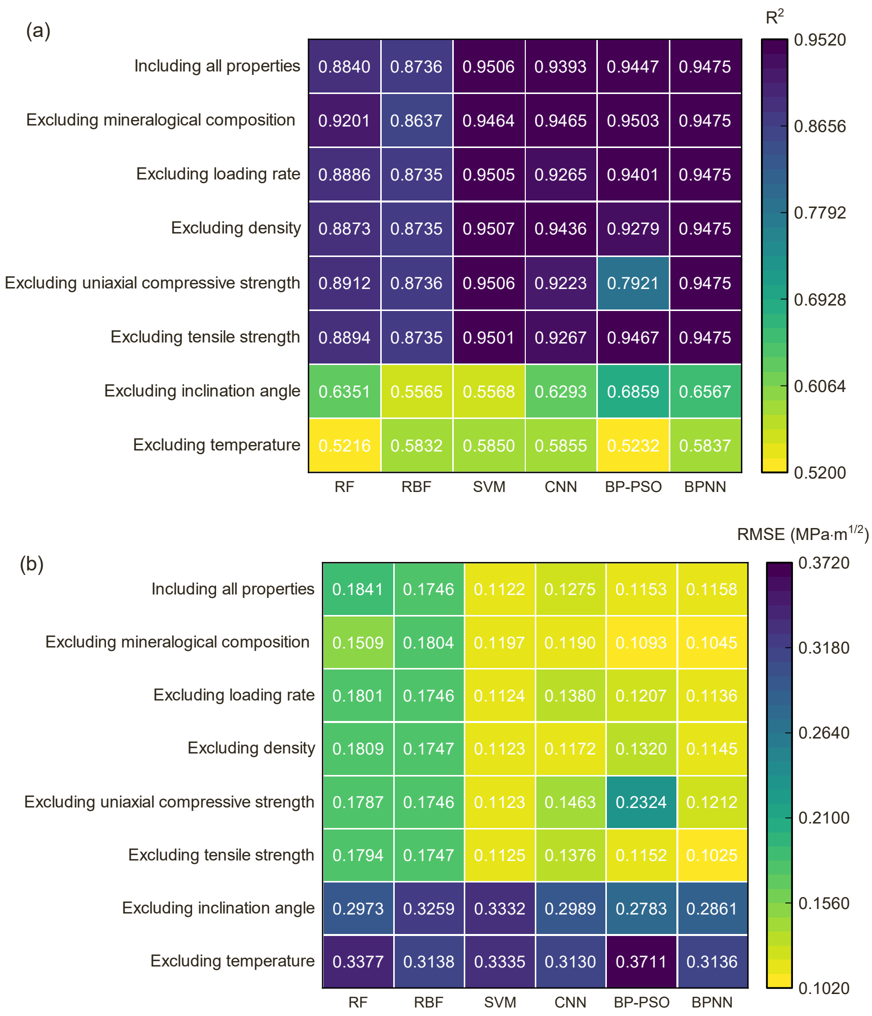

Fig. 7. Performance evaluation for six ML-based models with different groups of input variables. **a** coefficient of determination (R^2); **b** root mean square error (RMSE).

high temperature. For example, simply adding a large number of input variables will only slowdown the ML-based models [26]. Consequently, this section aims to comprehensively investigate the factors that impact prediction accuracy and highlight the significance of model parameters in predicting RFT.

4.1. Factors influencing prediction accuracy

The predictive performance of ML-based models is primarily influenced by four crucial factors as identified by Tian et al. [21]: (a) availability of a sufficient training dataset, (b) appropriate selection of hyperparameters, (c) utilization of effective training methods, and (d) suitable data preprocessing techniques. In this study, a comprehensive database comprising 297 samples is established, and the data is normalized before training. Considering the availability of the data, the number of samples taken in this work is also more abundant than many previous studies on predicting the RFT at room temperature [20,35,37,38,40]. Moreover, an iterative trial-and-error approach is adopted to optimize the hyperparameters of all six ML models. The obtained results demonstrate that models configured with these optimized hyperparameters exhibit favorable predictive performance on both the training and testing datasets (Fig. 5 and Table 4).

In addition to the aforementioned four factors associated with ML models itself, which significantly influence the predictive outcomes, there exist additional sources linked to the research problem concerning the temperature-dependent RFT that also impact the accuracy of predictions. The errors may arise from two sources: (a) different response mechanisms of RFT to temperature, and (b) inherent heterogeneity of rocks. The former results in a multitude of potential variations as different rock types exhibit diverse RFT variations and response mechanisms at different temperature levels. In this study, a comprehensive dataset encompassing four rock types, namely granite, mudstone, sandstone, and gypsum rock, was collected. Furthermore, even for a specific rock type, the variation pattern of RFT may change across different temperature ranges. For example, Hu et al. [7] observed that the mode I RFT of granite increases gradually from room temperature to 200 °C, and then it decreases when the temperature exceeds 200 °C. Moreover, the thermal expansion of different minerals in rocks is also closely related to the temperature. In practice, the mechanical properties (e.g., RFT, strength and modulus) of different rocks are improved or degraded over a range of temperatures depending not only on the conditions of thermally-induced microcracks but also on the level of thermal expansion [16]. Consequently, these factors contribute to intricate variations in the RFT at different temperatures. The latter issue represents a fundamental concern in problems related to rock prediction. RFT is closely related to rock heterogeneity, including property heterogeneity (e.g., strength and modulus) and microstructure heterogeneity (e.g., mineral type and grain size). In this work, due to limitations in data availability, the property heterogeneity was characterized using uniaxial compressive strength and tensile strength, while the microstructure heterogeneity was described based on mineralogical composition and density (Fig. 3). Nevertheless, these descriptors alone do not sufficiently capture the complete heterogeneity of rocks. It is undeniable that the ML-based models can deal with many geotechnical engineering problems with complex internal connections (i.e., rock thermodynamics problems in this work), but this is based on the rich data to describe the problem. Since our dataset cannot correctly describe the exact heterogeneity of every rock sample may leading to the errors in the prediction of RFT for some samples, even though three performance metrics (R^2, RMSE and MAE) show that the ML-predicted results are still accurate (Table 4). The establishment of more extensive datasets holds promise for enhancing the accuracy of predicting RFT, representing a compelling avenue for future research.

4.2. The necessity of model input variables

It is necessary to discuss in depth why the variables can affect the prediction of RFT. The model input variables in this work can be divided into two groups: external environment and internal factors.

4.2.1. External environment

4.2.1.1. Temperature. The influence of temperature on the RFT exhibits a complex behavior without clear regularity. It is widely acknowledged that subjecting rocks to sufficiently high temperatures (e.g., 1000 °C) leads to a reduction in RFT. However, within the lower temperature range (e.g., from room temperature to 200 °C), the effect of temperature treatment on RFT can either result in an increase or decrease [6,7]. For instance, previous studies by Meredith and Atkinson [54] indicated an increase in RFT between 20 and 100 °C, followed by a decrease for temperatures exceeding 100 °C. The observed increase in RFT during the lower temperature stage can be attributed to the closure of microcracks due to mineral expansion [55].

4.2.1.2. Loading rate. The mechanical properties of rocks exhibit clear differences between the static and dynamic loading conditions, which means that the loading rate has an effect on the mechanical properties. Although the loading rate in this work (0.012–1 mm/min) falls within the quasi-static loading range, it is noteworthy that further increases in loading rate can result in changes to the RFT. Yin et al. [56] found that the RFT increases almost linearly with increasing loading rates at different temperatures. Oh et al. [57] conducted an analysis of crack patterns generated in granite under static and dynamic loading conditions, revealing that cracks formed under static loading exhibited greater irregularity compared to those generated under dynamic loading. This observation highlights the disparity in the fracturing process and the associated RFT under different loading rates. Despite its relatively lower score in the feature importance evaluation (Fig. 6a), the loading rate remains a significant input variable for predicting the RFT at varying temperatures.

4.2.2. Internal factors

4.2.2.1. Sample radius, sample thickness, notch length and span length. The fundamental geometry parameters of a SCB specimen (Fig. 2) include the sample radius, sample thickness, notch length and span length. Previous studies [58] have demonstrated the notable impact of geometry effect on RFT through experimental investigations. For example, the mode I RFT of SCB specimen decreases with increasing the span length and it increases with increasing the sample thickness [58]. These findings can be attributed to the direct influence of specimen geometry on the stress distribution within the sample and the development of the fracture process zone ahead of the notch tip.

4.2.2.2. Inclination angle. The failure mode of SCB specimens is controlled by the inclination angle of notch [6]. When the inclination angle is set to 0°, the notch tip is only subjected to normal stress and it is under pure mode I. However, as the inclination angle increases, the notch tip may be subjected to a combination of normal and shear stresses (mode III) or pure shear stress (mode II). Therefore, the measured RFT of the rock varies with different inclination angles. Mode I RFT can be either higher or lower than mode II RFT, depending on the T-stress, as demonstrated by Wei et al. [59] and Li et al. [60]. And the ratio of mode I and mode II RFT changes with temperature [6,14]. According to the feature importance analysis, both the inclination angle and temperature hold nearly equal significance in predicting RFT (Fig. 6a).

4.2.2.3. Mineralogical composition and density. Mineralogical composition is one of the important components of microstructure of rock materials [61]. The RFT of different type of minerals are different, for example, the RFT of quartz (~5.34 MPa·$m^{1/2}$) are greater than that of K-feldspar (~4.83 MPa·$m^{1/2}$) and plagioclase (~2.70 MPa·$m^{1/2}$) [62]. Therefore, rock compositions with higher quartz content tend to possess greater RFT. Additionally, for the quartz-rich rocks (e.g., granite and sandstone in this work), the phase transformation of the primary component-quartz is a crucial factor to consider. Previous investigations have indicated that quartz undergoes a change from the α phase to the β phase at around 573 °C, resulting in volume expansion [19]. These changes in rock microstructure at different temperatures profoundly impact the RFT.

There is also a relationship between the density of rock and its RFT. The density and porosity have a high negative correlation, reflecting the mineral composition comprising the rock, as well as the level of cementation and compaction [21]. Furthermore, a higher content of high-density minerals (e.g., quartz) within the rock corresponds to an elevated RFT, underscoring the potential significance of rock density in predicting RFT. For example, previous studies have reported a linear or power-law relationship between rock density and RFT [63,64].

4.2.2.4. Uniaxial compressive strength and tensile strength. Uniaxial compressive strength and tensile strength are the fundamental mechanical properties. It has been found that the mode I RFT, uniaxial compressive strength and tensile strength of rock are correlated with each other [65]. Generally, rocks with higher tensile strength have stronger ability to resist crack initiation and propagation when subjected to tensile stress, resulting in higher RFT. This observation finds support in the similarity between the fractured surface of a specimen tested for tensile strength and that of a fracture toughness specimen. It is plausible that an inherent relationship exists between RFT, tensile strength and uniaxial compressive strength of rocks.

4.3. Applications, limitations, and future works

RFT is one of the most important index properties which dictate how a fracture will propagate during hydraulic fracturing, rock blast, tunneling, caving etc. Therefore, temperature-dependent RFT is very important for successful design, implementation and execution of deep geotechnical engineering structures, such as deep disposal of high-level radioactive nuclear waste and deep resources mining. Hence, a fast and accurate assessment of temperature-dependent RFT is required in both the field and laboratory. For example, in deep geotechnical engineering, the environmental temperature varies for rocks at different burial depths. This necessitates the knowledge of RFT at arbitrary temperatures in structural design, enabling more precise structural design. However, conducting an infinite number of RFT measurements at different temperatures in the laboratory is impractical due to the time-consuming and cost involved. Nevertheless, the proposed ML-based RFT prediction in this work can effectively address this issue. It is capable of reasonably predicting and extrapolating RFT values at different temperatures from limited experimental data. This significantly reduces experimental costs and facilitates faster and more accurate design of deep geotechnical engineering structures.

Nevertheless, this work had its limitations. More future work is needed to improve the prediction model. First, other additional features that have not been considered may also influence RFT, such as mineral grain size [66] and heating rate [67]. For example, Zhang et al. [66] found that the fracture toughness of Beishan granitic rock increases with the decrease of mineral grain size. These potential features can be incorporated into ML-based models in future work to predict RFT more accurately. Second, in addition to PSO, there are many optimization algorithms for hyperparameters selection, such as grid search, genetic algorithm, ant colony algorithm, and differential evolution [68,69]. These optimization algorithms may be more effective in the selection of the hyperparameters. Third, K-fold cross-validation approach can be used to enhance the generalization and credibility of the model. It reduces the evaluation bias introduced by random dataset splits and captures the model's stability and generalization ability more effectively [27]. Finally, the development of physics-guided ML is also a good topic. ML models purely built on data are often agnostic of the underlying physical processes (e.g., the material-microstructure-mechanical property relationships), which leads to inability to produce physically consistent results with limited available training data. Hence, the integration of prior physical knowledge into

ML-based models has recently been explored [70,71]. Therefore, physics-guided ML models will be developed in future work to improve the accuracy and reliability of the temperature-dependent RFT prediction models.

5. Conclusion

This work focused on the application of ML-based models in rock mechanics to accurately predict the RFT under different temperature conditions. A comprehensive investigation was conducted using six ML-based models, namely SVM, CNN, RF, BPNN, BP-PSO, and RBF. Training and testing were performed using a dataset comprising 297 samples. The results demonstrate that the SVM-based model performs better than the CNN, RF, BPNN, BP-PSO, and RBF models. For the testing dataset, the RMSE, MAE and R^2 values of SVM-based model are 0.1122 $MPa{\cdot}m^{1/2}$, 0.0829 $MPa{\cdot}m^{1/2}$ and 0.9506, respectively. The findings highlight temperature and inclination angle as the most significant input variables for reliably predicting RFT, as evidenced by their highest feature importance ranking values of 0.19833 and 0.15622, respectively. Moreover, mineralogical composition, density, uniaxial compressive strength and tensile strength also have an important influence on the prediction of temperature-dependent RFT. These findings make notable contributions to the field of rock mechanics, providing valuable insights into the factors influencing RFT under different temperature conditions. Furthermore, the study demonstrates the efficacy and potential of ML-based models in enhancing the accuracy and dependability of temperature-dependent RFT predictions, which can have important applications in the design and construction of geotechnical engineering structures.

Declaration of Competing Interest

The authors declare that they have no known competing financial interests or personal relationships that could have appeared to influence the work reported in this paper.

Data Availability

Data will be made available on request.

Acknowledgements

The authors are grateful to the National Natural Science Foundation of China (51778575) for the financial support. The authors also thank the editor and anonymous reviewers very much for their valuable advices.

Appendix A. Supporting information

Supplementary data associated with this article can be found in the online version at doi:10.1016/j.cscm.2023.e02622.

References

[1] G. Feng, Y. Kang, T. Meng, Y.Q. Hu, X.H. Li, The influence of temperature on mode I fracture toughness and fracture characteristics of sandstone, Rock. Mech. Rock. Eng. 50 (2017) 2007–2019, https://doi.org/10.1007/s00603-017-1226-y.
[2] S. Miao, P.Z. Pan, P. Yu, S. Zhao, C. Shao, Fracture analysis of Beishan granite after high-temperature treatment using digital image correlation, Eng. Fract. Mech. 225 (2020), 106847, https://doi.org/10.1016/j.engfracmech.2019.106847.
[3] T. Yin, Y. Wu, Q. Li, C. Wang, B. Wu, Determination of double-K fracture toughness parameters of thermally treated granite using notched semi-circular bending specimen, Eng. Fract. Mech. 226 (2020), 106865, https://doi.org/10.1016/j.engfracmech.2019.106865.
[4] X. Hu, H. Hu, N. Xie, Y. Huang, P. Guo, X. Gong, The effect of grain size heterogeneity on mechanical and microcracking behavior of pre-heated Lac du Bonnet granite using a grain-based model, Rock. Mech. Rock. Eng. 56 (2023) 5923–5954, https://doi.org/10.1007/s00603-023-03381-5.
[5] X. Hu, Y. Qi, H. Hu, G. Lei, N. Xie, X. Gong, A micromechanical-based failure criterion for rocks after high-temperature treatment, Eng. Fract. Mech. 284 (2023), 109275, https://doi.org/10.1016/j.engfracmech.2023.109275.
[6] M. Alneasan, A.K. Alzo'ubi, Temperature effect on the fracture behavior of granite under three loading modes (I, I/II, and II), Rock. Mech. Rock. Eng. 56 (3) (2023) 2197–2211, https://doi.org/10.1007/s00603-022-03149-3.
[7] Y. Hu, Y. Hu, P. Jin, G. Zhao, Z. Zhao, C. Li, Real-time mode-I fracture toughness and fracture characteristics of granite from 20 °C to 600 °C, Eng. Fract. Mech. 277 (2023), 109001, https://doi.org/10.1016/j.engfracmech.2022.109001.
[8] M.D. Kuruppu, Y. Obara, M.R. Ayatollahi, K.P. Chong, T. Funatsu, ISRM-suggested method for determining the mode I static fracture toughness using semi-circular bend specimen, Rock. Mech. Rock. Eng. 47 (2014) 267–274, https://doi.org/10.1007/s00603-013-0422-7.
[9] S.H. Chang, C.I. Lee, S. Jeon, Measurement of rock fracture toughness under modes I and II and mixed-mode conditions by using disc-type specimens, Eng. Geol. 66 (1–2) (2002) 79–97, https://doi.org/10.1016/S0013-7952(02)00033-9.
[10] M.R. Ayatollahi, J. Akbardoost, Size and geometry effects on rock fracture toughness: mode I fracture, Rock. Mech. Rock. Eng. 47 (2014) 677–687, https://doi.org/10.1007/s00603-013-0430-7.
[11] W. Yao, Y. Xu, K. Xia, S. Wang, Dynamic mode II fracture toughness of rocks subjected to confining pressure, Rock. Mech. Rock. Eng. 53 (2020) 569–586, https://doi.org/10.1007/s00603-019-01929-y.
[12] T. Funatsu, M. Kuruppu, K. Matsui, Effects of temperature and confining pressure on mixed-mode (I–II) and mode II fracture toughness of Kimachi sandstone, Int. J. Rock. Mech. Min. Sci. 67 (2014) 1–8, https://doi.org/10.1016/j.ijrmms.2013.12.009.
[13] P. Kang, L. Hong, Y. Fazhi, Z. Quanle, S. Xiao, L. Zhaopeng, Effects of temperature on mechanical properties of granite under different fracture modes, Eng. Fract. Mech. 226 (2020), 106838, https://doi.org/10.1016/j.engfracmech.2019.106838.

[14] M. Alneasan, A.K. Alzo'ubi, M. Behnia, O. Mughieda, Experimental observations on the effect of thermal treatment on the crack speed and mode I and II fracture toughness in brittle and ductile rocks, Theor. Appl. Fract. Mech. 121 (2022), 103525, https://doi.org/10.1016/j.tafmec.2022.103525.
[15] N.A. Al-Shayea, K. Khan, S.N. Abduljauwad, Effects of confining pressure and temperature on mixed-mode (I–II) fracture toughness of a limestone rock, Int. J. Rock. Mech. Min. Sci. 37 (4) (2000) 629–643, https://doi.org/10.1016/S1365-1609(00)00003-4.
[16] G. Feng, C. Zhu, X. Wang, S. Tang, Thermal effects on prediction accuracy of dense granite mechanical behaviors using modified maximum tangential stress criterion, J. Rock. Mech. Geotech. Eng. 15 (2022) 1, https://doi.org/10.1016/j.jrmge.2022.12.003.
[17] T.Y. Guo, L.N.Y. Wong, Z. Wu, Microcracking behavior transition in thermally treated granite under mode I loading, Eng. Geol. 282 (2021), 105992, https://doi.org/10.1016/j.enggeo.2021.105992.
[18] J. Wu, J. Gao, Z. Feng, S. Chen, T. Nie, Investigation of fracture process zone properties of mode I fracture in heat-treated granite through digital image correlation, Eng. Fract. Mech. 235 (2020), 107192, https://doi.org/10.1016/j.engfracmech.2020.107192.
[19] Y. Feng, H. Su, L. Yu, C. Wu, H. Wang, Mixed mode I-II fracture mechanism of sandstone samples after thermal treatment: Insights from optical monitoring and thermal analysis, Theor. Appl. Fract. Mech. 125 (2023), 103883, https://doi.org/10.1016/j.tafmec.2023.103883.
[20] D.G. Roy, T.N. Singh, J. Kodikara, Predicting mode-I fracture toughness of rocks using soft computing and multiple regression, Measurement 126 (2018) 231–241, https://doi.org/10.1016/j.measurement.2018.05.069.
[21] Y. Tian, F. Zhou, L. Hu, X. Tang, H. Liu, Optimization of rock mechanical properties prediction model based on block database, Rock. Mech. Rock. Eng. (2023) 1–24, https://doi.org/10.1007/s00603-023-03378-0.
[22] D. Guha Roy, T.N. Singh, J. Kodikara, M. Talukdar, Correlating the mechanical and physical properties with mode-I fracture toughness of rocks, Rock. Mech. Rock. Eng. 50 (2017) 1941–1946, https://doi.org/10.1007/s00603-017-1196-0.
[23] M.D. Wei, F. Dai, N.W. Xu, Y. Liu, T. Zhao, A novel chevron notched short rod bend method for measuring the mode I fracture toughness of rocks, Eng. Fract. Mech. 190 (2018) 1–15, https://doi.org/10.1016/j.engfracmech.2017.11.041.
[24] M. Wei, F. Dai, Y. Liu, A. Li, Z. Yan, Influences of loading method and notch type on rock fracture toughness measurements: from the perspectives of T-stress and fracture process zone, Rock. Mech. Rock. Eng. 54 (2021) 4965–4986, https://doi.org/10.1007/s00603-021-02541-9.
[25] Y. Hu, Y. Hu, G. Zhao, P. Jin, Z. Zhao, C. Li, Experimental investigation of the relationships among P-wave velocity, tensile strength, and mode-I fracture toughness of granite after high-temperature treatment, Nat. Resour. Res. 31 (2) (2022) 801–816, https://doi.org/10.1007/s11053-022-10020-3.
[26] A. Baghbani, T. Choudhury, S. Costa, J. Reiner, Application of artificial intelligence in geotechnical engineering: A state-of-the-art review, Earth-Sci. Rev. 228 (2022), 103991, https://doi.org/10.1016/j.earscirev.2022.103991.
[27] O. Kolawole, R.H. Assaad, Modeling and prediction of temporal biogeomechanical properties using novel machine learning approach, Rock. Mech. Rock. Eng. (2023) 1–21, https://doi.org/10.1007/s00603-023-03353-9.
[28] B.H.Z. Sami, B.F.Z. Sami, P. Kumar, A.N. Ahmed, G.E. Amieghemen, M.M. Sherif, A. El-Shafie, Feasibility analysis for predicting the compressive and tensile strength of concrete using machine learning algorithms, Case Stud. Constr. Mater. 18 (2023), e01893, https://doi.org/10.1016/j.cscm.2023.e01893.
[29] M. Wang, G. Zhao, W. Liang, N. Wang, A Comparative Study on the development of Hybrid SSA-RF and PSO-RF Models for Predicting the Uniaxial Compressive Strength of Rocks, Case Stud. Constr. Mater. (2023), e02191, https://doi.org/10.1016/j.cscm.2023.e02191.
[30] I.U. Ekanayake, D.P.P. Meddage, U. Rathnayake, A novel approach to explain the black-box nature of machine learning in compressive strength predictions of concrete using Shapley additive explanations (SHAP), Case Stud. Constr. Mater. 16 (2022), e01059, https://doi.org/10.1016/j.cscm.2022.e01059.
[31] X. Hu, J. Shentu, N. Xie, Y. Huang, G. Lei, H. Hu, X. Gong, Predicting triaxial compressive strength of high-temperature treated rock using machine learning techniques, J. Rock. Mech. Geotech. Eng. (2022) 1–11, https://doi.org/10.1016/j.jrmge.2022.10.014.
[32] J. de-Prado-Gil, C. Palencia, N. Silva-Monteiro, R. Martínez-García, To predict the compressive strength of self compacting concrete with recycled aggregates utilizing ensemble machine learning models, Case Stud. Constr. Mater. 16 (2022), e01046, https://doi.org/10.1016/j.cscm.2022.e01046.
[33] J. Tie, W. Meng, M. Wei, W. Wu, Loading rate and mineralogical controls on tensile strength of rocks: A machine learning view, Rock. Mech. Rock. Eng. (2023) 1–7, https://doi.org/10.1007/s00603-023-03354-8.
[34] Y.T. Wang, X. Zhang, X.S. Liu, Machine learning approaches to rock fracture mechanics problems: Mode-I fracture toughness determination, Eng. Fract. Mech. 253 (2021), 107890, https://doi.org/10.1016/j.engfracmech.2021.107890.
[35] B. Afrasiabian, M. Eftekhari, Prediction of mode I fracture toughness of rock using linear multiple regression and gene expression programming, J. Rock. Mech. Geotech. Eng. 14 (5) (2022) 1421–1432, https://doi.org/10.1016/j.jrmge.2022.03.008.
[36] A. Dehestani, F. Kazemi, R. Abdi, M. Nitka, Prediction of fracture toughness in fibre-reinforced concrete, mortar, and rocks using various machine learning techniques, Eng. Fract. Mech. 276 (2022), 108914, https://doi.org/10.1016/j.engfracmech.2022.108914.
[37] E. Emami Meybodi, S.K. Hussain, M. Fatehi Marji, V. Rasouli, Application of machine learning models for predicting rock fracture toughness mode-I and mode-II, J. Min. Environ. 13 (2) (2022) 465–480, https://doi.org/10.22044/JME.2022.11596.2148.
[38] A. Mahmoodzadeh, H.R. Nejati, M. Mohammadi, H.H. Ibrahim, M. Khishe, S. Rashidi, H.F.H. Ali, Prediction of Mode-I rock fracture toughness using support vector regression with metaheuristic optimization algorithms, Eng. Fract. Mech. 264 (2022), 108334, https://doi.org/10.1016/j.engfracmech.2022.108334.
[39] A. Mahmoodzadeh, D. Fakhri, A.H. Mohammed, A.S. Mohammed, H.H. Ibrahim, S. Rashidi, Estimating the effective fracture toughness of a variety of materials using several machine learning models, Eng. Fract. Mech. (2023), 109321, https://doi.org/10.1016/j.engfracmech.2023.109321.
[40] A.I. Lawal, S. Kwon, Reliability assessment of empirical equations, ANN and MARS models for predicting the mode I fracture toughness from non-destructive rock properties, Rock. Mech. Rock. Eng. (2023) 1–10, https://doi.org/10.1007/s00603-023-03345-9.
[41] B. Mahanta, T.N. Singh, P.G. Ranjith, Influence of thermal treatment on mode I fracture toughness of certain Indian rocks, Eng. Geol. 210 (2016) 103–114, https://doi.org/10.1016/j.enggeo.2016.06.008.
[42] G. Feng, Y. Kang, F. Chen, Y.W. Liu, X.C. Wang, The influence of temperatures on mixed-mode (I+II) and mode-II fracture toughness of sandstone, Eng. Fract. Mech. 189 (2018) 51–63, https://doi.org/10.1016/j.engfracmech.2017.07.007.
[43] G. Feng, X.C. Wang, Y. Kang, S.G. Luo, Y.Q. Hu, Effects of temperature on the relationship between mode-I fracture toughness and tensile strength of rock, Appl. Sci. 9 (7) (2019) 1326, https://doi.org/10.3390/app9071326.
[44] C. Li, Y. Hu, T. Meng, C. Zhang, R. Gao, P. Jin, Y. Hu, Mode-I fracture toughness and mechanisms of Salt-Rock gypsum interlayers under real-time high-temperature conditions, Eng. Fract. Mech. 240 (2020), 107357, https://doi.org/10.1016/j.engfracmech.2020.107357.
[45] J. Liu, L. Chen, C. Wang, K. Man, L. Wang, J. Wang, R. Su, Characterizing the mechanical tensile behavior of Beishan granite with different experimental methods, Int. J. Rock. Mech. Min. Sci. 69 (2014) 50–58, https://doi.org/10.1016/j.ijrmms.2014.03.007.
[46] A. Farhadian, E. Ghasemi, S.H. Hoseinie, R. Bagherpour, Development of a new test method for evaluating the abrasivity of granite building stones during polishing process based on weight loss of abrasive tool, Constr. Build. Mater. 303 (2021), 124497, https://doi.org/10.1016/j.conbuildmat.2021.124497.
[47] M. Alneasan, A.K. Alzo'ubi, Extensive experimental investigation on the effect of thermal treatment and lateral pressure on the shear behavior of intact mudstone, Sci. Rep. 13 (1) (2023), 6820, https://doi.org/10.1038/s41598-023-33841-5.
[48] K. Breede, K. Dzebisashvili, X. Liu, G. Falcone, A systematic review of enhanced (or engineered) geothermal systems: past, present and future, Geotherm. Energy 1 (2013) 1–27, https://doi.org/10.1186/2195-9706-1-4.
[49] L. Huang, J. Li, H. Hao, X. Li, Micro-seismic event detection and location in underground mines by using Convolutional Neural Networks (CNN) and deep learning, Tunn. Undergr. Space Technol. 81 (2018) 265–276, https://doi.org/10.1016/j.tust.2018.07.006.
[50] W. Zhang, C. Wu, H. Zhong, Y. Li, L. Wang, Prediction of undrained shear strength using extreme gradient boosting and random forest based on Bayesian optimization, Geosci. Front. 12 (1) (2021) 469–477, https://doi.org/10.1016/j.gsf.2020.03.007.
[51] L. Breiman, Random forests, Mach. Learn. 45 (2001) 5–32.
[52] S.M. Lundberg, S.I. Lee, A unified approach to interpreting model predictions, Adv. Neural Inf. Process. Syst. (2017) 4765–4774.
[53] D. Wang, S. Thunéll, U. Lindberg, L. Jiang, J. Trygg, M. Tysklind, Towards better process management in wastewater treatment plants: Process analytics based on SHAP values for tree-based machine learning methods, J. Environ. Manag. 301 (2022), 113941, https://doi.org/10.1016/j.jenvman.2021.113941.

[54] P.G. Meredith, B.K. Atkinson, Fracture toughness and subcritical crack growth during high-temperature tensile deformation of Westerly granite and Black gabbro, Phys. Earth Planet. Inter. 39 (1) (1985) 33–51, https://doi.org/10.1016/0031-9201(85)90113-X.

[55] M.R. Balme, V. Rocchi, C. Jones, P.R. Sammonds, P.G. Meredith, S. Boon, Fracture toughness measurements on igneous rocks using a high-pressure, high-temperature rock fracture mechanics cell, J. Volcanol. Geotherm. Res. 132 (2–3) (2004) 159–172, https://doi.org/10.1016/S0377-0273(03)00343-3.

[56] T. Yin, X. Li, K. Xia, S. Huang, Effect of thermal treatment on the dynamic fracture toughness of Laurentian granite, Rock. Mech. Rock. Eng. 45 (2012) 1087–1094, https://doi.org/10.1007/s00603-012-0240-3.

[57] S.W. Oh, G.J. Min, S.W. Park, M.S. Kim, Y. Obara, S.H. Cho, Anisotropic influence of fracture toughness on loading rate dependency for granitic rocks, Eng. Fract. Mech. 221 (2019), 106677, https://doi.org/10.1016/j.engfracmech.2019.106677.

[58] L. Tutluoglu, C.K. Batan, M.R.M. Aliha, Tensile mode fracture toughness experiments on andesite rock using disc and semi-disc bend geometries with varying loading spans, Theor. Appl. Fract. Mech. 119 (2022), 103325, https://doi.org/10.1016/j.tafmec.2022.103325.

[59] M.D. Wei, F. Dai, N.W. Xu, Y. Liu, T. Zhao, Fracture prediction of rocks under mode I and mode II loading using the generalized maximum tangential strain criterion, Eng. Fract. Mech. 186 (2017) 21–38, https://doi.org/10.1016/j.engfracmech.2017.09.026.

[60] Y. Li, F. Dai, M. Wei, H. Du, Numerical investigation on dynamic fracture behavior of cracked rocks under mixed mode I/II loading, Eng. Fract. Mech. 235 (2020), 107176, https://doi.org/10.1016/j.engfracmech.2020.107176.

[61] X. Hu, P. Guo, N. Xie, H. Hu, G. Lei, J. Ma, X. Gong, Creep behavior and associated acoustic characteristics of heterogeneous granite containing a single pre-existing flaw using a grain-based parallel-bonded stress corrosion model, Rock. Mech. Rock. Eng. 56 (2023) 4799–4832, https://doi.org/10.1007/s00603-023-03291-6.

[62] X.Y. Liu, D.P. Xu, S.J. Li, S.L. Qiu, Q. Jiang, An insight into the mechanical and fracture characterization of minerals and mineral interfaces in granite using nanoindentation and micro X-ray computed tomography, Rock. Mech. Rock. Eng. (2023) 1–17, https://doi.org/10.1007/s00603-023-03221-6.

[63] G.J. Brown, D.J. Reddish, Experimental relations between rock fracture toughness and density, Int. J. Rock. Mech. Min. Sci. Geomech. Abstr. 34 (1) (1997) 153–155, https://doi.org/10.1016/S1365-1609(97)80042-1.

[64] D. Guha Roy, T.N. Singh, J. Kodikara, M. Talukdar, Correlating the mechanical and physical properties with mode-I fracture toughness of rocks, Rock. Mech. Rock. Eng. 50 (2017) 1941–1946, https://doi.org/10.1007/s00603-017-1196-0.

[65] Z.X. Zhang, An empirical relation between mode I fracture toughness and the tensile strength of rock, Int. J. Rock. Mech. Min. Sci. 39 (3) (2002) 401–406, https://doi.org/10.1016/S1365-1609(02)00032-1.

[66] H. Zhang, L. Chen, J. Liu, Y. Li, J. Wang, Influence of Grain Size and Saturation on the Fracture Toughness of Granitic Rocks, Rock. Mech. Rock. Eng. 55 (12) (2022) 7881–7886, https://doi.org/10.1007/s00603-022-03006-3.

[67] Q. Li, X. Li, T. Yin, Effect of microwave heating on fracture behavior of granite: An experimental investigation, Eng. Fract. Mech. 250 (2021), 107758, https://doi.org/10.1016/j.engfracmech.2021.107758.

[68] H. Huang, J. Chang, D. Zhang, J. Zhang, H. Wu, G. Li, Machine learning-based automatic control of tunneling posture of shield machine, J. Rock. Mech. Geotech. Eng. 14 (4) (2022) 1153–1164, https://doi.org/10.1016/j.jrmge.2022.06.001.

[69] C. Fan, N. Zhang, B. Jiang, W.V. Liu, Using deep neural networks coupled with principal component analysis for ore production forecasting at open-pit mines, J. Rock. Mech. Geotech. Eng. (2023), https://doi.org/10.1016/j.jrmge.2023.06.005.

[70] X. Li, X. Ma, F. Xiao, C. Xiao, F. Wang, S. Zhang, A physics-constrained long-term production prediction method for multiple fractured wells using deep learning, J. Pet. Sci. Eng. 217 (2022), 110844, https://doi.org/10.1016/j.petrol.2022.110844.

[71] G.E. Karniadakis, I.G. Kevrekidis, L. Lu, P. Perdikaris, S. Wang, L. Yang, Physics-informed machine learning, Nat. Rev. Phys. 3 (6) (2021) 422–440, https://doi.org/10.1038/s42254-021-00314-5.